Response of Idealized Baroclinic Wave Life Cycles to Stratospheric Flow Conditions

TORBEN KUNZ, KLAUS FRAEDRICH, AND FRANK LUNKEIT

Meteorologisches Institut, Universität Hamburg, Hamburg, Germany

(Manuscript received 30 April 2008, in final form 6 January 2009)

ABSTRACT

Dynamical stratosphere–troposphere coupling through a response of baroclinic waves to lower stratospheric flow conditions is investigated from an initial value approach. A series of adiabatic and frictionless nonlinear baroclinic wave life cycles in a midlatitude tropospheric jet with different initial zonal flow conditions in the stratosphere is simulated, using a dry primitive equation model with spherical geometry. When a stratospheric jet, located at various latitudes between 35° and 70°, is removed from the initial conditions, the wavenumber-6 life cycle behavior changes from the well-known LC1 to LC2 evolution, characterized by anticyclonic and cyclonic wave breaking, respectively. Linear theory, in terms of refractive index and the structure of the corresponding fastest-growing normal mode, is found to be unable to explain this stratosphere-induced LC1 to LC2 transition. This implies that altered nonlinear wave–mean flow interactions are important. The most significant stratosphere-induced change that extends into the nonlinear baroclinic growth stage is a region of downward wave propagation in the lower stratosphere associated with positive values of the squared refractive index near 20 km. Furthermore, it is demonstrated that the difference between the response of the tropospheric circulation to LC1 and LC2 life cycles closely resembles the meridional and vertical structure of the North Atlantic Oscillation (NAO), with positive (negative) NAO-like anomalies being driven by LC1 (LC2). Thus, a weakened stratospheric jet induces the generation of negative NAO-like anomalies in the troposphere, consistent with the observed stratosphere–NAO connection.

1. Introduction

Dynamical coupling of the extratropical wintertime stratosphere with the underlying troposphere increasingly appears as an important aspect of both tropospheric extended-range (intraseasonal) weather forecasts (e.g., Baldwin and Dunkerton 2001; Thompson et al. 2002; Baldwin et al. 2003; Charlton et al. 2004) and climate variability on interannual and longer time scales (e.g., Labitzke and van Loon 1988; Baldwin et al. 1994; Perlwitz and Graf 1995; Thompson and Wallace 1998; Baldwin et al. 2007). Although many studies focus on the impact of stratospheric variability on the tropospheric annular mode, evidence exists that the largest tropospheric response is associated with the North Atlantic Oscillation (NAO), which shifts into the negative phase when the stratospheric polar night jet is weakened, and vice versa (Baldwin et al. 1994; Ambaum and Hoskins 2002; Scaife et al. 2005).

Corresponding author address: Torben Kunz, Meteorologisches Institut, Universität Hamburg, Bundesstraße 55, D-20146 Hamburg, Germany.
E-mail: torben.kunz@zmaw.de

DOI: 10.1175/2009JAS2827.1

Different processes are involved in dynamical stratosphere–troposphere coupling, such as downward control by the zonal mean meridional circulation due to anomalous stratospheric planetary wave forcing (Haynes et al. 1991; Thompson et al. 2006) or downward planetary wave reflection in the stratosphere (Perlwitz and Harnik 2003). However, observational and modeling studies also suggest the possibility of a downward influence from the lower stratosphere by direct modulation of tropospheric baroclinic, that is, synoptic-scale waves (Baldwin and Dunkerton 1999, 2001; Baldwin et al. 2003; Kushner and Polvani 2004; Charlton et al. 2004; Wittman et al. 2004, 2007), which largely contribute to the growth and decay of tropospheric low-frequency modes such as the NAO (e.g., Feldstein 2003).

In particular, from the synoptic viewpoint of Benedict et al. (2004), Franzke et al. (2004), and Rivière and Orlanski (2007), it is suggested that the positive (negative) phase of the NAO emerges from synoptic-scale anticyclonic (cyclonic) wave breaking in the North Atlantic storm-track region, although low-frequency eddies also contribute to its growth and decay (Feldstein 2003). Here, the terms anticyclonic and cyclonic wave breaking are used to describe the dynamical evolution during the barotropic decay stage of the two distinctly different idealized baroclinic wave life cycles, usually referred to as LC1 and LC2, respectively, found by Simmons and Hoskins (1980) and further investigated by Thorncroft et al. (1993) and Hartmann and Zuercher (1998), among others. These life cycles differ significantly in terms of eddy momentum fluxes during the nonlinear stage and the associated changes of the zonal mean flow. Specifically, the LC1 (LC2) life cycle induces a poleward (equatorward) shift of the midlatitude jet, which results in a zonal mean zonal flow configuration that resembles the poleward (equatorward) displacement of the North Atlantic eddy-driven jet during the positive (negative) phase of the NAO (as seen in Ambaum et al. 2001).

Furthermore, observed tropospheric synoptic-scale waves frequently extend into the lower stratosphere, as shown by Canziani and Legnani (2003). Therefore, it is highly suggestive that the flow at these levels may interact with those waves and, through subsequent changes in the baroclinic wave life cycle behavior (and thus the wave breaking characteristics), may affect the NAO in the troposphere. The issue of whether baroclinic wave life cycles respond to lower stratospheric flow conditions in terms of an LC1–LC2 transition has already been considered by Wittman et al. (2007). In the present paper, we revisit this question with similar techniques but with less simplified initial flows. Specifically, to address this question, a series of adiabatic and frictionless nonlinear baroclinic wave life cycle simulations is carried out with a dry primitive equation model with spherical geometry, using different initial zonal flow conditions in the stratosphere.

The paper is organized as follows: The model and experimental setup are presented in section 2. Section 3 investigates the response of the baroclinic wave life cycles to the different stratospheric initial flow conditions, and its potential relevance to the NAO is discussed in section 4. Conclusions and further discussion follow in section 5.

2. Model and experimental setup

a. Model

For the numerical simulation of idealized nonlinear baroclinic wave life cycles in this study we use the dry primitive equation Portable University Model of the Atmosphere (PUMA; Fraedrich et al. 1998, 2005).[1] Such simplified general circulation models provide a platform for a systematic analysis of the dynamics of planetary atmospheres under idealized conditions, with minimal computational expenses allowing for extensive sensitivity studies. Here, we integrate this model with T42 spectral horizontal resolution, 30 σ levels in the vertical, and a time step of 15 min. The model levels are nonequally distributed in the vertical (as in Polvani and Kushner 2002; see their appendix) and the Simmons and Burridge (1981) vertical difference scheme is used. The uppermost model level is then located at about 85 km. The model is integrated in the adiabatic and frictionless mode, apart from a horizontal eighth-order (∇^8) hyperdiffusion with a dissipation time scale of 6 h on the smallest resolved scale. All simulations are symmetric about the equator.

b. Experimental setup

Each simulation is characterized by the configuration of the initial zonal flow conditions, given by a prescribed zonally uniform and purely zonal flow, which is in thermal wind balance (see the appendix for details of the balancing procedure). Because we want to study the impact of a stratospheric jet on midlatitude baroclinic waves, the initial conditions set up a polar night jet in the stratosphere and a baroclinically unstable jet in the troposphere at 45° latitude. At this latitude the baroclinically unstable jet is representative of the observed eddy-driven jet in the North Atlantic storm-track region during winter, in contrast to the jet near 30°N in the North Pacific sector.

The potentially most dramatic changes in baroclinic life cycle behavior are to be expected to arise from an LC1–LC2 transition. In previous studies on baroclinic life cycle behavior, such a transition was induced by adding barotropic cyclonic shear about the unstable jet in the initial conditions (e.g., Thorncroft et al. 1993; Hartmann and Zuercher 1998). Accordingly, in the real atmosphere, changes between LC1- and LC2-like behavior of observed baroclinic waves can be associated with equivalent barotropic shear anomalies about the midlatitude jet, related to tropospheric variability modes such as the NAO or Northern Annular Mode (e.g., Ambaum et al. 2001; Lorenz and Hartmann 2003). Hartmann (2000) studied the relative contributions of lower versus upper tropospheric cyclonic shear leading to the transition, and shear confined to the lower troposphere was found to be most efficient in that idealized life cycle study. Here, we can exploit this result for the setup of our model simulations. Because we want to study the impact of the stratospheric jet on baroclinic life cycles, a lower tropospheric cyclonic shear of varying strength, centered about the unstable jet in the troposphere, is added as a third component to the initial flow setup. Thus, in the context of the present study, this is merely a device to control life cycle behavior by a

[1] Model code and users' guide are freely available online (http://www.mi.uni-hamburg.de/puma).

single parameter (the shear parameter; see below) and to bring the system close to the LC1–LC2 transition point without changing the stratospheric flow at the same time.

Consequently, the initial zonal flow u is specified as follows:

$$\begin{aligned} u(\phi, z) &= u_T(\phi, z) + u_S(\phi, z) + u_{\mathrm{CS}}(\phi, z) \\ &= U_T h_T(\phi) v_T(z) + U_S h_S(\phi) v_S(z) \\ &\quad + U_{\mathrm{CS}} h_{\mathrm{CS}}(\phi) v_{\mathrm{CS}}(z), \end{aligned} \tag{1}$$

with latitude ϕ and height $z = -H\ln(p/p_0)$ (where 7 km is the approximate scale height H of an isothermal atmosphere at $T = 240$ K and $p_0 = 1013.25$ hPa); the subscripts T, S, and CS refer to the tropospheric jet, stratospheric jet, and the lower tropospheric cyclonic shear, respectively.[2]

The horizontal and vertical profiles are given by (written for a single hemisphere)

$$h_T(\phi) = \sin^3(\pi \sin^2\phi), \tag{2}$$

$$h_S(\phi) = \begin{cases} \cos^2\left(\dfrac{\pi}{2}\dfrac{\phi - \phi_S}{\Delta\phi_S}\right) & \text{if } |\phi - \phi_S| < \Delta\phi_S \\ 0 & \text{otherwise} \end{cases}, \tag{3}$$

$$h_{\mathrm{CS}}(\phi) = \exp\left[-\left(\frac{\phi - \phi_l}{\Delta\phi_{\mathrm{CS}}}\right)^2\right] - \exp\left[-\left(\frac{\phi - \phi_h}{\Delta\phi_{\mathrm{CS}}}\right)^2\right], \text{ and} \tag{4}$$

$$v_T(z) = \frac{z}{z_{\mathrm{Tmax}}}\exp\left\{\frac{1}{\alpha}\left[1 - \left(\frac{z}{z_{\mathrm{Tmax}}}\right)^{\alpha}\right]\right\}, \quad \alpha = 5, \tag{5}$$

$$v_S(z) = \begin{cases} \sin^2\left(\dfrac{\pi}{2}\dfrac{z - z_{\mathrm{Sbot}}}{z_{\mathrm{Smax}} - z_{\mathrm{Sbot}}}\right), & \text{if } z_{\mathrm{Sbot}} < z < 2z_{\mathrm{Smax}} - z_{\mathrm{Sbot}}, \\ 0, & \text{otherwise,} \end{cases} \tag{6}$$

$$v_{\mathrm{CS}}(z) = \begin{cases} \cos^2\left(\dfrac{\pi}{2}\dfrac{z}{z_{\mathrm{CSmax}}}\right), & \text{if } z < z_{\mathrm{CSmax}}, \\ 0, & \text{otherwise,} \end{cases} \tag{7}$$

with $z_{\mathrm{Tmax}} = 11$ km, $z_{\mathrm{Smax}} = 50$ km, $z_{\mathrm{Sbot}} = 8$ km, $\Delta\phi_S = 20°$ latitude, $\Delta\phi_{\mathrm{CS}} = 12.5°$ latitude, $\phi_l = 30°$ latitude, $\phi_h = 60°$ latitude, $z_{\mathrm{CSmax}} = 9$ km, and $U_T = 45$ m s^{-1}. The following three parameters are varied to set up the initial zonal flow for the different simulations: The strength of the lower tropospheric cyclonic shear is controlled by the shear parameter U_{CS}, the amplitude of the stratospheric jet by U_S, and its latitudinal position by ϕ_S. The initial zonal flow for selected configurations is shown in Fig. 1. The vertical profile of the horizontally averaged temperature corresponds to the *U.S. Standard Atmosphere, 1976* (COESA 1976).

Next, an unbalanced small-amplitude (4 Pa) surface pressure perturbation (concentrated to midlatitudes) of a single zonal wavenumber $s = 6$ is added to the initial zonal flow to excite the growth of a baroclinically unstable wave in the tropospheric jet. The sensitivity of the results to the zonal wavenumber is tested by additional simulations with $s = 5$ and $s = 7$. The model is integrated over a period of 30 days (60 days for $s = 5$) to simulate a complete nonlinear baroclinic wave life cycle. Note that because of the nonlinearity of the model, higher harmonics (multiples of s) are excited during the life cycle simulations.

Two sets of simulations are carried out, with and without a stratospheric jet (respectively denoted by S75, with $U_S = 75$ m s^{-1} and $\phi_S = 60°$ latitude, and by S00, with $U_S = 0$ m s^{-1}). Each set contains 18 simulations with different shear parameter values (denoted by T00 to T10, with $U_{\mathrm{CS}} = 0$, 1, 2, 3, 4, 5, 6, 6.5, 6.75, 7, 7.25, 7.5, 7.75, 8, 8.25, 8.5, 9, 10 m s^{-1}). A simulation without a stratospheric jet and with $U_{\mathrm{CS}} = 7.25$ m s^{-1}, for example, is then referred to as S00T07.25. Additional sets of simulations are set up to study the sensitivity to the latitudinal position of the stratospheric jet ($\mathrm{S75}_{25°}$ to $\mathrm{S75}_{70°}$, with $\phi_S = 25°, \ldots, 70°$ latitude at steps of 5° latitude). Note that for legibility the standard case with the stratospheric jet at its approximate climatological position ($\phi_S = 60°$ latitude) is denoted by S75 without an index.

Additionally, a breeding scheme is used to compute the fastest-growing normal mode for the initial zonal flow of some key simulations (see next section). This allows for an exact comparison of normal mode structures for different initial flow conditions. For this purpose, a model integration is performed with an initial flow and an $s = 6$ surface pressure perturbation as described above for the nonlinear life cycle simulations, but in addition (i) the amplitude of the zonally nonuniform components of the model fields is rescaled by a factor of 0.5 each time that the surface pressure amplitude

[2] The zonal wind $u(z)$ is transformed to model σ levels by assuming a constant surface pressure $p^* = p_0$. Subsequently, the wind field $u(\sigma)$ is used in the balancing procedure, and the obtained initial surface pressure field $p^*(t = 0)$ is, in general, not constant.

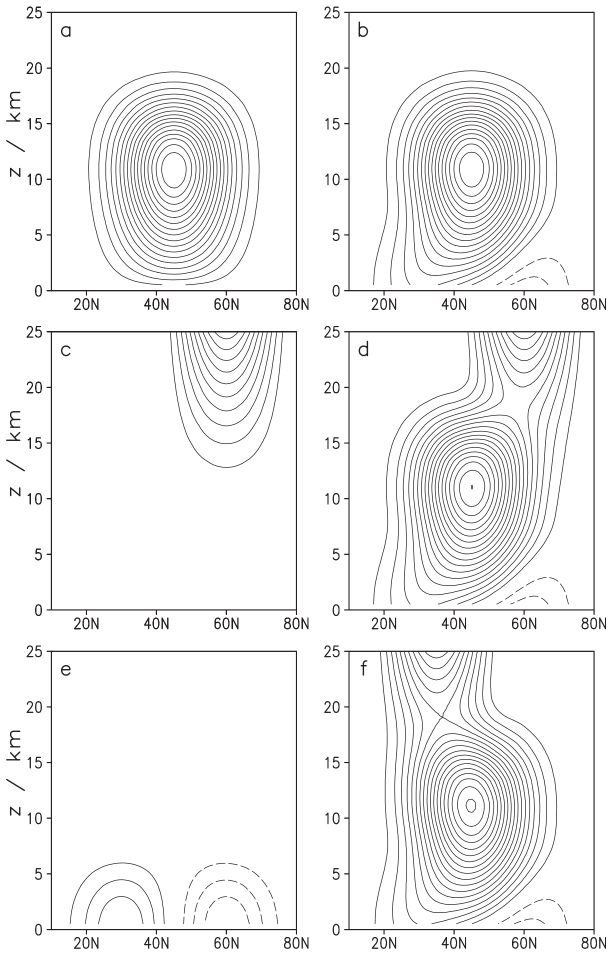

FIG. 1. Initial zonal flow components (a) $u_T(\phi,z)$, (c) $u_S(\phi,z)$ with $\phi_S = 60°$ latitude and $U_S = 75$ m s^{-1}, and (e) $u_{CS}(\phi,z)$ with $U_{CS} = 10$ m s^{-1}. Initial zonal flow for the simulations (a) S00T00, (b) S00T07.25, (d) S75T07.25, and (f) S75$_{35°}$T06.75. Contour interval is 2.5 m s^{-1}, the zero contour is omitted, and dashed contours indicate negative values.

exceeds 0.2 hPa, and (ii) zonal mean fields are kept constant at every time step. In all cases convergence is reached after less than 30 days.

3. Stratosphere-induced LC1–LC2 transition

A complete life cycle of a nonlinear baroclinic wave is simulated by all integrations of this study. These life cycles undergo the well-known sequence of baroclinic growth and subsequent barotropic decay, arising from the baroclinic conversion of eddy available potential energy into eddy kinetic energy (EKE) and from the barotropic conversion of EKE into zonal mean kinetic energy, respectively. The time series of both conversion terms and of EKE were calculated following Ulbrich and Speth (1991) and exhibit nonlinear life cycles with a time scale on the order of 10 days (not shown). The preceding linear stage lasts for about 9 days for zero initial shear and for about 12 days for strong initial shear (shear parameter $U_{CS} = 10$ m s^{-1}).[3]

The rest of this section is split into three parts. First, the LC1–LC2 transition, controlled by the lower tropospheric cyclonic shear, is illustrated for situations with and without a stratospheric jet in the initial conditions. Next, the impact of the stratospheric jet on baroclinic life cycles is analyzed by means of linear theory, and finally stratosphere-induced changes during the nonlinear stage are presented.

a. LC1–LC2 transition of life cycle behavior

When the shear parameter exceeds some critical value, a clear transition from LC1 to LC2 behavior of the wave is found for $s = 6$, which is also reflected in the time evolution of EKE in the sense that a significantly higher level of EKE is retained after the barotropic decay stage for LC2 life cycles compared to LC1 cases [consistent with Simmons and Hoskins (1980), Thorncroft et al. (1993), Hartmann and Zuercher (1998), and Hartmann (2000)]. Figure 2 shows maps of potential vorticity on an upper tropospheric isentrope (at $\theta = 325$ K) during the barotropic decay stage of an LC1 life cycle (S00T00), with the typical synoptic signature of anticyclonic wave breaking (AB), and of an LC2 life cycle (S00T10), which is accompanied by cyclonic wave breaking (CB). The associated equatorward (weak poleward) wave propagation during the barotropic decay stage of an LC1 (LC2) life cycle induces a poleward (equatorward) shift of the tropospheric jet, also including significant changes of surface winds (as in Hartmann and Zuercher 1998) and, thus, zonal mean surface pressure. The left panel of Fig. 3 shows the total change of zonal mean surface pressure as a function of latitude and the shear parameter U_{CS}. Evidently, a very sharp LC1–LC2 transition occurs between $U_{CS} = 6.5$ m s^{-1} and $U_{CS} = 6.75$ m s^{-1}. The LC1 life cycle induces a mass shift from poleward of 50° latitude to lower latitudes, whereas LC2 shifts mass from midlatitudes to lower and higher latitudes. For $s = 5$ ($s = 7$) all life cycle simulations result in LC1 (LC2) behavior. The induced change of zonal mean surface pressure for these life cycles (not shown) exhibits a virtually identical meridional profile to that of the respective LC1 and LC2 life cycles with $s = 6$. The occurrence of only LC1 and LC2 life cycles for $s = 5$ and $s = 7$, respectively, is further confirmed by the typical

[3] However, for life cycles with $s = 5$ and strong initial shear the linear stage lasts considerably longer. Because in these cases also the barotropic decay is largely delayed, the model needs to be integrated over more than 30 days for the corresponding nonlinear life cycles to complete.

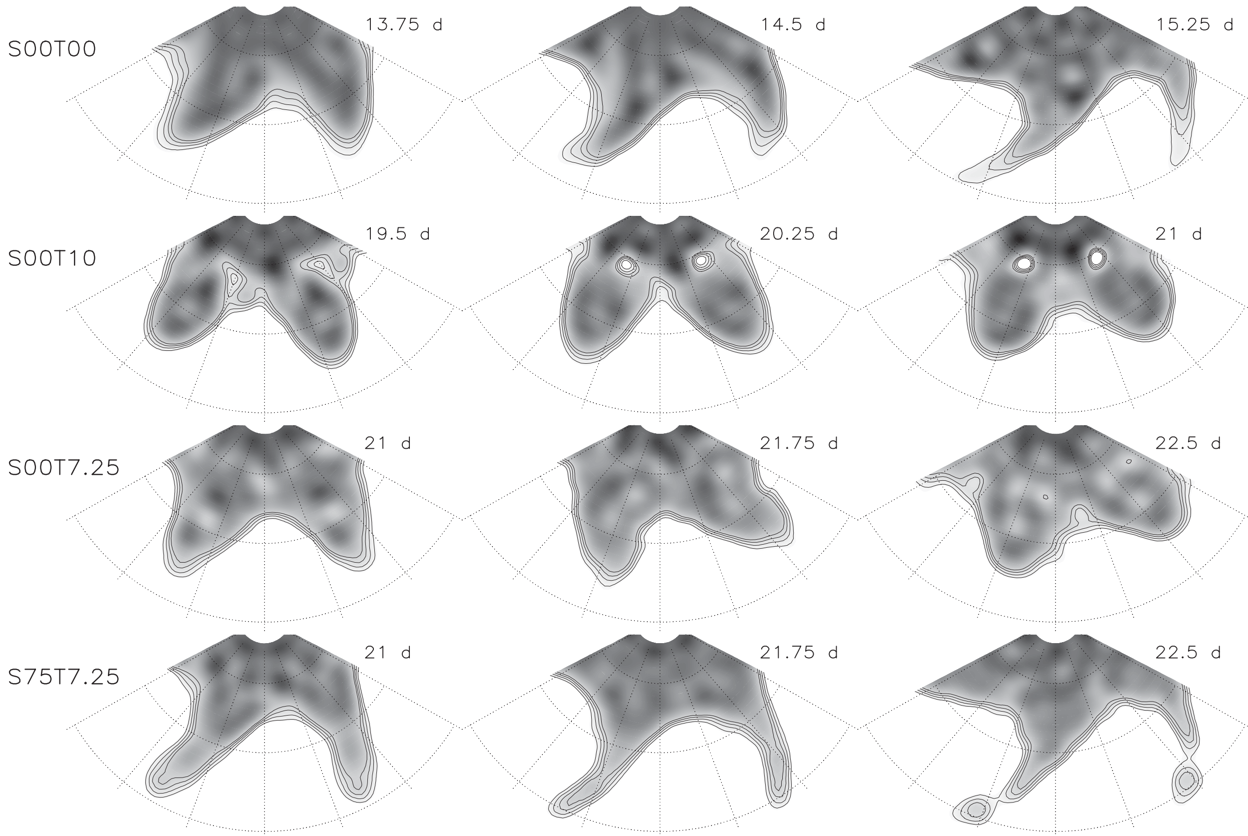

FIG. 2. Potential vorticity on the 325-K isentrope for the life cycles (top to bottom) S00T00, S00T10, S00T07.25, and S75T07.25 (right) at the time of maximum EKE decrease due to barotropic conversion and (middle) 18 and 36 h earlier; zonal wavenumber $s = 6$. Contours are shown at 2, 2.5, 3, and 3.5 PVU; darker shading represents larger values. The outermost latitude circle is plotted at 30°N.

differences in the EKE time series for these two life cycles as well as by isentropic potential vorticity maps. Because we are interested in the LC1–LC2 transition, only results from life cycles with $s = 6$ are presented in the remaining part of this study.

A very similar response to increased initial cyclonic shear is found when a stratospheric jet (at $\phi_S = 60°$ latitude) is introduced to the initial conditions, as can be inferred from the right panel of Fig. 3. Again, a sharp LC1–LC2 transition is evident. However, there is a distinct shift of the LC1–LC2 transition point to larger values of the shear parameter, and the transition occurs between $U_{\mathrm{CS}} = 7.75$ m s^{-1} and $U_{\mathrm{CS}} = 8$ m s^{-1}. Potential vorticity maps on the 325-K isentrope of two life cycles (S00T07.25 and S75T07.25; Fig. 2) within the stratosphere-sensitive regime (with respect to U_{CS}) do in fact exhibit clear LC1 and LC2 behavior during the barotropic decay stage, again associated with an AB and a CB event, respectively. Figure 4 shows the zonal mean zonal wind and the Eliassen–Palm (EP) flux for the same life cycles at the time of maximum barotropic decay, and the equatorward (poleward) wave propagation further confirms the occurrence of AB (CB) during the decay of the LC1 (LC2) life cycle.

Such a stratosphere-induced shift of the transition point also exists for other latitudinal positions of the

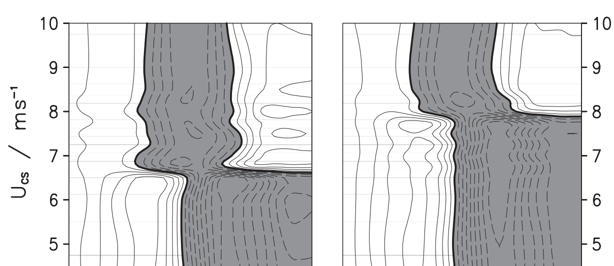

FIG. 3. Total change of zonal mean surface pressure during a life cycle, as a function of latitude and initial lower tropospheric cyclonic shear (the shear parameter U_{CS}, in m s^{-1}), for life cycles (left) without (S00T04. . .S00T10) and (right) with a stratospheric jet (S75T04. . .S75T10); zonal wavenumber $s = 6$. Contour interval is 10 hPa; dashed contours and shading indicate negative values.

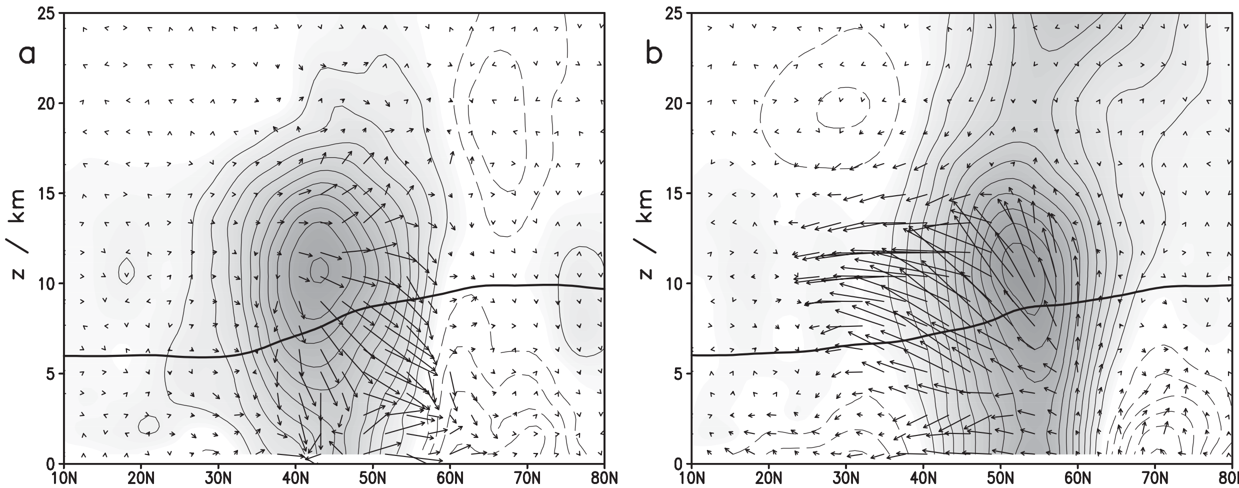

FIG. 4. Zonal mean zonal wind (thin contours, shading), 325K-isentrope (thick contour), and EP flux **F** (arrows) for life cycles (a) S00T07.25 and (b) S75T07.25, at the time of maximum EKE decrease due to barotropic conversion; zonal wavenumber $s = 6$. Dashed contours indicate negative values; the zero contour is omitted; contour interval is 5 m s^{-1}; darker shading indicates larger positive values. The EP flux is scaled by (p/p_0), with $p_0 = 1013.25$ hPa, to account for the decrease of density with height. Thus, the plotted quantity is $\mathbf{F} \times (p/p_0)^{-1}$. An arrow spanning 10° latitude (5-km height) interval represents a scaled EP flux of 2.09×10^9 Kg s^{-2} (9.40×10^6 Kg s^{-2}).

stratospheric jet. Table 1 specifies the maximum (minimum) shear parameter resulting in an LC1 (LC2) life cycle for different values of ϕ_S. Adding a stratospheric jet to the initial conditions leads to an LC2 to LC1 transition for $\phi_S = 70°, \ldots, 35°$ latitude. Note that in the latter case the stratospheric jet is located on the equatorward side of the tropospheric jet. The stratosphere-sensitive regime is maximized for $\phi_S = 65°, \ldots, 50°$ latitude, just where the observed stratospheric polar night jet has its climatological position. An opposite stratosphere-induced transition, from LC1 to LC2, only occurs when the stratospheric jet is added at rather unrealistically low latitudes ($\phi_S \leq 30°$ latitude).

In summary, by increasing the cyclonic shear in the troposphere (U_{CS}) beyond a critical value, a transition in life cycle behavior is obtained (for $s = 6$) from LC1, associated with anticyclonic wave breaking on the equatorward side of the jet, to LC2, associated with cyclonic wave breaking on the poleward side of the jet. When a stratospheric jet (U_S) is added at realistic latitudes, the transition occurs for larger values of tropospheric cyclonic shear. Consequently, the presence of the stratospheric jet favors LC1 behavior, whereas LC2 behavior is preferred in the absence of a stratospheric jet.

b. Linear analysis: Refractive index and normal modes

In previous life cycle studies, attempts have been made to explain the LC1–LC2 transition by using arguments of linear Rossby wave theory, although the sharpness of the transition has been attributed to effects of nonlinear dynamics (Hartmann and Zuercher 1998). In these studies the transition is induced by adding cyclonic shear in the troposphere. Thorncroft et al. (1993) demonstrate how this increases the distance of a subtropical critical line to the midlatitude wave, whereas Hartmann and Zuercher (1998) also find that stronger initial cyclonic shear increasingly hinders the growing wave to reduce this shear, which eventually leads to cyclonic wave breaking and thus LC2 behavior. In the context of the present study, this raises the question of whether linear theory can also help to understand the stratosphere-induced LC1–LC2 transition, found in the previous section.

As in the above studies, we calculate the refractive index for linear quasigeostrophic Rossby waves to investigate the effect of the stratospheric zonal flow on wave propagation characteristics. The squared refractive index for zonal wavenumber s, multiplied by the

TABLE 1. Maximum (minimum) shear parameter U_{CS}, in m s^{-1}, resulting in an LC1 (LC2) life cycle, for different latitudinal positions of the stratospheric jet ϕ_S. The last column specifies the case without a stratospheric jet (S00, with $U_S = 0$ m s^{-1}).

ϕ_S	70°	65°	60°	55°	50°	45°	40°	35°	30°	25°	S00
LC1 for $U_{CS} \leq$	7.50	7.75	7.75	7.75	7.75	7.50	7.25	6.75	6.00	6.00	6.50
LC2 for $U_{CS} \geq$	7.75	8.00	8.00	8.00	8.00	7.75	7.50	7.00	6.50	6.50	6.75

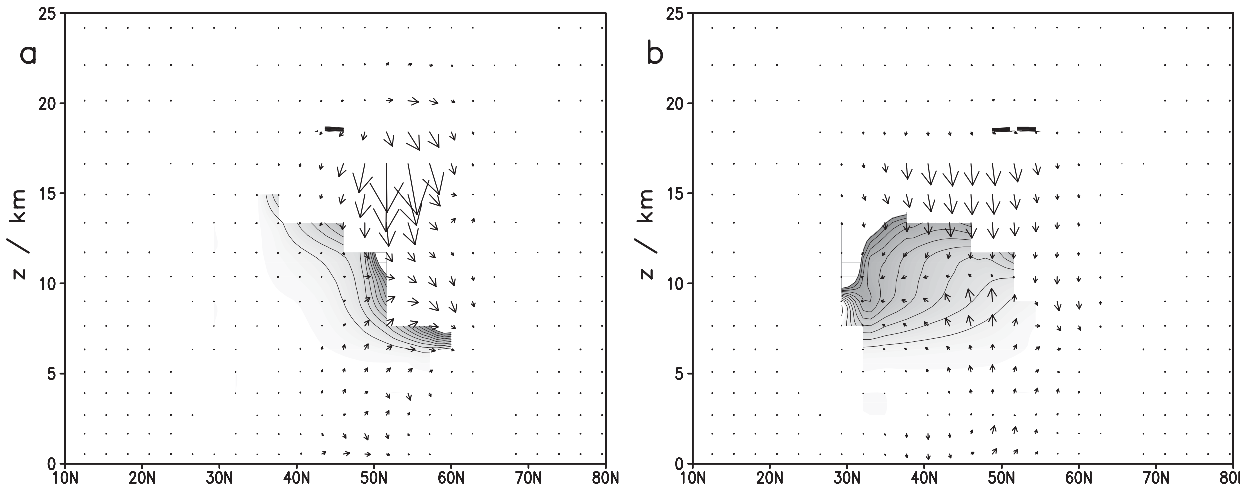

FIG. 5. Differences (a) S00T07.25 minus S75T07.25 and (b) S00T06.75 minus $S75_{35°}T06.75$ of refractive index an_6 (contours, shading) and scaled EP flux $\mathbf{F} \times (p/p_0)^{-1}$ (arrows arbitrary arrow length scale) of the corresponding fastest-growing normal mode. Contours are at 0.1, 0.2, . . . , 1.0; darker shading indicates larger positive values.

radius of the earth a, can be written as (Matsuno 1971; Andrews et al. 1987)

$$a^2 n_s^2 = \frac{a\overline{q}_\phi}{\overline{u} - ca\cos\phi} - \frac{s^2}{\cos^2\phi} - \frac{a^2 f^2}{4N^2 H^2}, \qquad (8)$$

using the modified quasigeostrophic potential vorticity equation to include the isallobaric contribution of the meridional wind in the planetary vorticity advection term [for details, see Matsuno (1970, 1971)], where

$$\overline{q}_\phi = 2\Omega\cos\phi - \left[\frac{(\overline{u}\cos\phi)_\phi}{a\cos\phi}\right]_\phi - \frac{a}{\rho_0}\left(\frac{\rho_0 f^2}{N^2}\overline{u}_z\right)_z \qquad (9)$$

is the meridional gradient of the zonal mean quasigeostrophic potential vorticity; $(\cdot)_\phi$ and $(\cdot)_z$ indicate the meridional and vertical derivative, respectively, and $\overline{(\cdot)}$ the zonal average, f is the Coriolis parameter, N the buoyancy frequency (of an isothermal atmosphere at $T = 240$ K), Ω the earth's rotation rate, ρ_0 the basic density, and c the eastward angular phase speed of the wave. The angular phase speed c is estimated as the eastward movement of the $s = 6$ component of the meridional wind at 500 hPa averaged between 46° and 55° latitude and from $t = 7$ days to $t = 9$ days.[4]

The effect of discarding the stratospheric jet at 60° latitude (S00T07.25 minus S75T07.25) on the refractive index (at $t = 0$) is shown in Fig. 5a, together with the difference in the EP flux $\mathbf{F}$ of the corresponding fastest-growing normal modes. In the upper troposphere and tropopause region, increased poleward refractive index gradients are obtained and, in accordance with linear theory, the normal mode EP flux signature, at those altitudes, exhibits an additional poleward component. By contrast, the opposite effect is found when the stratospheric jet is discarded at 35° latitude (S00T06.75 minus $S75_{35°}T06.75$; Fig. 5b), with increased equatorward refractive index gradients and (weak) EP flux component. However, because in both cases shown in Fig. 5 the removal of the stratospheric jet induces an LC1 to LC2 transition (Table 1), which is always associated with significant additional poleward wave propagation during the late nonlinear stage, we can conclude that these linear arguments do not explain the stratosphere-induced LC1–LC2 transition. Note that Wittman et al. (2007) also find that linear theory is unable to explain their transition in life cycle behavior.

The most distinct feature, however, is the additional downward EP flux signature in the lower stratosphere between 14 and 18 km when the stratospheric jet is removed (Figs. 5a,b).[5] This is associated with the shallow propagation region (a region where $a^2 n_6^2 > 0$, indicated by shading in Fig. 6) between 18 and 20 km, which largely disappears in the presence of a stratospheric jet (Figs. 6a and 6b for S00T07.25 and S75T07.25, respectively), as does the downward EP flux signature below. Although the refractive index concept is not

[4] During this period c varies by not more than 5% of its mean value.

[5] This additional downward EP flux signature is also found for all other latitudinal positions of the stratospheric jet used in this study.

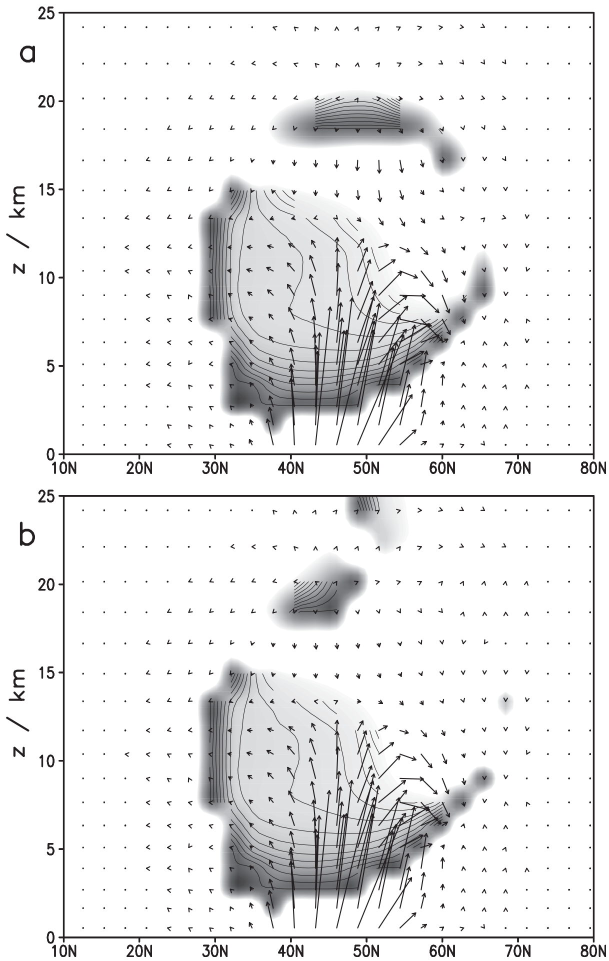

FIG. 6. Refractive index an_6 (thin contours; interval 1; highest contour is plotted at 14) and region of positive refractive index squared $a^2n_6^2 > 0$ (shading; darker shading indicates larger values; darkest shading appears near critical lines where $\overline{u} = ca\cos\phi$) of initial zonal flow for (a) S00T07.25 and (b) S75T07.25. Also included is the scaled EP flux $\mathbf{F} \times (p/p_0)^{-1}$ (arrows) of the corresponding fastest-growing normal mode. Arrow lengths are reduced by a factor of 5 compared to Fig. 5.

valid because the vertical scale of this propagation region is much smaller than that of the wave [and hence the Wentzel–Kramers–Brillouin–Jeffries (WKBJ) approximation does not apply], Fig. 6a suggests the presence of wave activity near that region, which might be interpreted as the signature of a counterpropagating Rossby wave (see, e.g., Heifetz et al. 2004) located in that region, where $\overline{q}_\phi < 0$ and $\overline{u} - ca\cos\phi < 0$, and which interacts with the waves at the tropopause and the surface. Although the counterpropagating Rossby wave perspective is based on the linearized potential vorticity equation, it is shown to explain well the phase speed of baroclinic wave life cycles far into the nonlinear stage (Methven et al. 2005).

c. Nonlinear stage: Stratosphere-induced changes above and near the tropopause

A similar downward propagation signature in the midlatitude lower stratosphere between 14 and 18 km as a response to a removed stratospheric jet still exists during the nonlinear baroclinic growth stage of the life cycle. The difference S00T07.25 minus S75T07.25 (S00T06.75 minus $S75_{35°}T06.75$) of the total change until the time of maximum baroclinic conversion of both the EP flux and the zonal mean meridional wind is presented in Fig. 7a (Fig. 7b) and shows a downward EP flux in that region and, additionally, poleward meridional flow above and equatorward flow below near the tropopause. Here, a 30-h average is applied as a filter to both quantities to remove the very high-frequency variations in the troposphere with a time scale of a few hours. The patterns of the vertical EP flux and the meridional wind are very similar irrespective of the latitudinal position of the discarded stratospheric jet and appear just above the baroclinically unstable jet. By contrast, this is not the case for the horizontal EP flux component, with additional poleward (weak equatorward) propagation between 45° and 60° latitude (30° and 45° latitude) when the stratospheric jet is removed at 60° (35°) latitude, similar to differences during the linear stage.

Similarly, the response of the zonal mean zonal wind to the removal of a stratospheric jet from the initial conditions significantly depends on the latitudinal position of the jet (Figs. 7c,d). Additional cyclonic shear of equivalent barotropic character between 40° and 60° latitude occurs throughout the troposphere when a stratospheric jet is removed at 60° latitude (Fig. 7c), closely resembling the final zonal mean zonal wind response after the complete life cycle (Fig. 7e), whereas anticyclonic shear confined to the tropopause region follows when the jet is removed at 35° latitude (Fig. 7d). However, because in the latter case the final response (Fig. 7f) is again an additional equivalent barotropic cyclonic shear in the troposphere, it is implied that the zonal mean zonal wind changes—even during the nonlinear baroclinic growth stage—do not indicate whether a stratosphere-induced transition occurs. Thus wave–mean flow interactions during the nonlinear stage are expected to play an important role.

These results suggest that stratosphere-induced changes to the linear stage in terms of the initial zonal flow (refractive index) and normal mode structure, as well as subsequent differences, partly extending into the nonlinear baroclinic growth stage, may only help to explain the much larger (smaller) stratosphere-sensitive regime in the case of a stratospheric jet located on the poleward (equatorward) side of the unstable jet in the

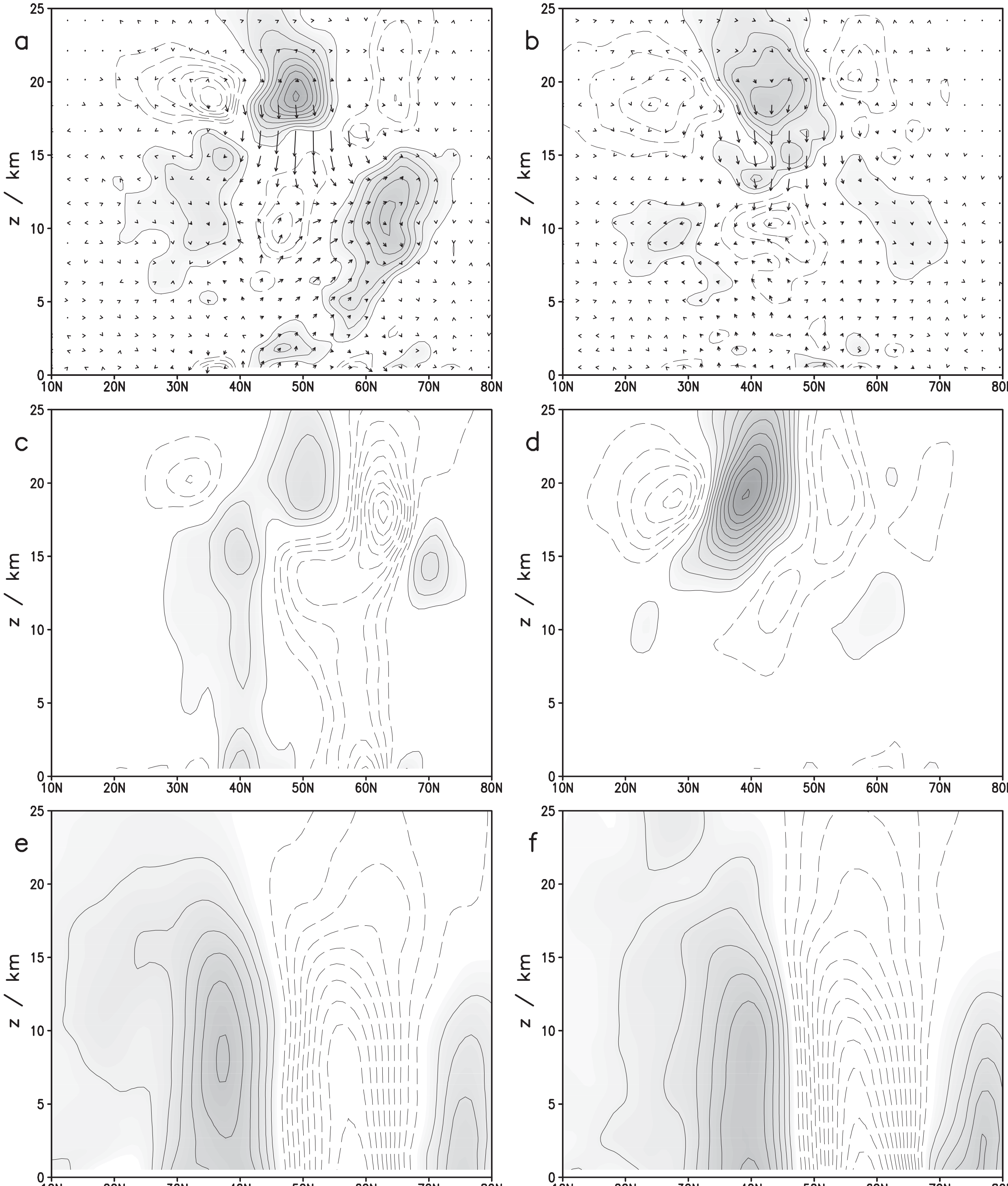

FIG. 7. Differences (left) S00T07.25 minus S75T07.25 and (right) S00T06.75 minus $S75_{35°}T06.75$ of (a),(b) total change of zonal mean meridional wind (contours, shading) and scaled EP flux $\mathbf{F} \times (p/p_0)^{-1}$ (arrows) until the time of maximum EKE production (at $t = 16.5$ days) due to baroclinic conversion. (c),(d) As in (a),(b), but for zonal mean zonal wind. (e),(f) As in (c),(d), but for total change until the end of the barotropic decay stage (at about $t = 24$ days). Dashed contours indicate negative values; the zero contour is omitted; contour interval is (a),(b) 0.05, (c),(d) 0.5, and (e),(f) 5 m s^{-1}; darker shading indicates larger positive values. Arrow lengths in (a),(b) are scaled as in Fig. 4. A 30-h average centered around $t = 16.5$ days is used in (a)–(d), and an average over the last 5 days ($t = 25, \ldots, 30$ days) in (e) and (f).

troposphere. The additional downward propagation in the midlatitude lower stratosphere (and induced meridional circulation), however, appears to be a feature of this model setup, independent of the latitudinal position of the stratospheric jet in the initial conditions. Thus, future investigation is necessary to analyze the mechanism by which stratosphere-induced altered nonlinear wave–mean flow interactions affect baroclinic wave life cycle behavior, involving baroclinic processes in the lower stratosphere as found in this study. Also, nonlinear wave activity conservation diagnostics—as applied, for example, by Thorncroft et al. (1993) and Magnusdottir and Haynes (1996)—are expected to provide additional insights into the relevant dynamics, including nonlinear advection of wave activity by the meridional circulation.

Finally, it is worth mentioning that the shallow propagation region (where $a^2n_6^2 > 0$, with $\overline{q}_\phi < 0$ and $\overline{u} - ca\cos\phi < 0$) in the lower stratosphere in cases without a stratospheric jet (see, e.g., Fig. 6a), associated with the aforementioned downward EP flux signature below it, is not found when the refractive index is calculated for the zonal mean zonal flow averaged between the end of the linear stage and the end of the nonlinear barotropic decay stage. Consistently, this propagation region is not expected to appear in zonal and time mean zonal flows obtained from long forced-dissipative model simulations or observational data, which represent an average over several baroclinic life cycles. Rather, that region should be interpreted as a feature intrinsic to highly baroclinically unstable states of the tropospheric jet, associated with negative meridional potential vorticity gradients $\overline{q}_\phi < 0$ (mainly due to large vertical zonal wind curvature $\partial^2\overline{u}/\partial z^2 > 0$ above the tropospheric jet maximum) at lower stratospheric levels where $\overline{u} - ca\cos\phi < 0$. Hence, such states may occur intermittently and locally in regions of increased baroclinicity, most probably within the storm tracks.

4. Baroclinic wave breaking and its relation to the NAO

In this section we discuss the relevance of the previously described stratosphere-induced shift of the LC1–LC2 transition point for the connection between the NAO and the stratosphere. As presented in other life cycle studies and in the previous section, the response of the zonal mean circulation to an LC1 life cycle (i.e., the total change during the cycle) differs significantly from the response to an LC2 life cycle, as shown, for example, in Fig. 3 for the zonal mean surface pressure. Within either the LC1 or LC2 regime, the response to an individual life cycle is quite robust, and large changes occur only near the sharp LC1–LC2 transition. This is also true for the response of the zonal mean 300-hPa geopotential height (not shown), although at this upper tropospheric level (near 9 km) the response to LC1 life cycles is exactly 180° out of phase with the LC2 response. As shown by Hartmann and Zuercher (1998), the changes of the zonal mean circulation during baroclinic life cycles are largely driven by meridional wave propagation during the barotropic decay stage, associated with either anticyclonic (for LC1) or cyclonic baroclinic wave breaking (for LC2).

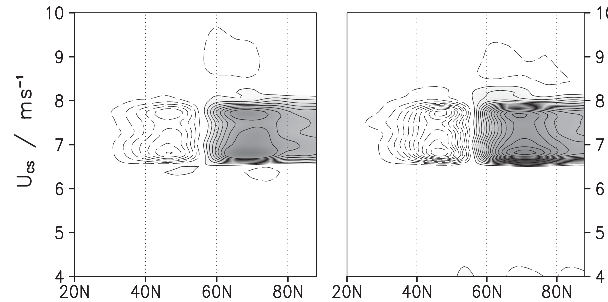

FIG. 8. (left) Difference S00 minus S75 of the total change of zonal mean surface pressure during a life cycle, as a function of latitude and initial lower tropospheric cyclonic shear (the shear parameter U_{CS}, in m s^{-1}). Contour interval is 10 hPa. This corresponds to the difference between the left and right panels of Fig. 3. (right) The same, but for zonal mean 300-hPa geopotential height. Contour interval is 50 gpm. Dashed contours indicate negative values; the zero contour is omitted; darker shading indicates larger positive values.

Because several studies suggest a close connection between the two kinds of wave breaking and the opposite phases of the NAO, it is interesting to look at the difference between the response of the circulation to LC1 and LC2 life cycles. Figure 8 shows the difference between the response to life cycles with and without a stratospheric jet; the left (right) panel represents the difference between the left and right panel of Fig. 3 for surface pressure (for 300-hPa geopotential height). Within the stratosphere-sensitive regime (with respect to the shear parameter) where, consequently, the LC1 response is subtracted from the LC2 response, a distinct meridional dipole pattern is found[6], and this meridional profile is very similar to that of the observed NAO pattern with its zero point near 55° latitude [for reference see, e.g., Ambaum et al. (2001, their Fig. 4)]. Also, the virtually identical structure of the patterns at lower and upper tropospheric levels (Fig. 8) matches the equivalent barotropic structure of the NAO. This illustrates how the successive occurrence of AB and CB

[6] Note that the difference between any LC2 and LC1 response results in virtually the same meridional pattern: for example, S00T07.25 minus S00T06 or S75T08 minus S75T07.25, where cases with identical stratospheric flow conditions are subtracted.

events may drive an equivalent barotropic NAO-like variability mode in a region of frequent wave breaking, as is the case for the North Atlantic storm-track region, if the baroclinically unstable jet at 45° latitude in our model setup is assumed to be representative of the observed eddy-driven jet in the North Atlantic sector. In this picture, the positive (negative) phase of the NAO is expected to prevail during episodes when the eddy-driven jet is in the LC1 (LC2) regime, associated with the occurrence of AB (CB) events. This is consistent with the abovementioned NAO–wave breaking view (Benedict et al. 2004; Rivière and Orlanski 2007; Woollings et al. 2008).

Clearly, life cycles with different initial cyclonic shear also have different initial zonal mean surface pressure distributions, since the cyclonic shear component of our model setup has its maximum at the surface. This might appear as a rather unrealistic feature of the highly idealized simulations of the present study, when compared to observed variability modes of midlatitude zonal flows with maximum amplitudes in the upper troposphere. However, (i) both kinds of wave breaking are frequently observed in the North Atlantic storm-track region (as a clear indication of LC1- and LC2-like baroclinic wave behavior), which implies that the mean state of the North Atlantic eddy-driven jet is indeed close to an LC1–LC2 transition point; and (ii) the respective response to LC1 and LC2 life cycles is found to be robust against different specific model setups used in different life cycle studies (cf., e.g., Thorncroft et al. 1993; Hartmann 2000; Orlanski 2003). This strongly suggests that just those life cycle simulations that are close to the LC1–LC2 transition point—say, with $U_{CS} = 6, \ldots, 8\ \mathrm{m\ s^{-1}}$ (with only small differences in the initial surface pressure distribution)—are most relevant to the real atmosphere in the NAO–wave breaking context.

The above discussion implies a possible mechanism for the observed connection between the stratospheric annular mode or the polar night jet and the NAO through a direct modulation of tropospheric baroclinic processes by the lower stratospheric flow conditions. Specifically, our results suggest that a strong (weak) stratospheric polar night jet favors anticyclonic (cyclonic) wave breaking in the troposphere, which tends to shift the NAO into the positive (negative) phase. This is consistent with Baldwin et al. (1994), who find a close relation between observed winter mean stratospheric zonal winds and an NAO-like variability mode in the troposphere, and also with the positive correlation between the NAO and the stratospheric polar vortex found by Ambaum and Hoskins (2002) in monthly and daily data. Blessing et al. (2005) also provide related observational evidence.

As mentioned in the introduction, Wittman et al. (2004, 2007) also interpret their results in the context of stratosphere–troposphere coupling (although the tropospheric response to baroclinic wave breaking is associated with the surface annular mode or Arctic oscillation rather than the NAO). However, there are considerable differences in comparison with the present study:

(i) Whereas Wittman et al. (2004), using an experimental setup that basically corresponds to our S75T00 case, essentially find synoptic-scale changes in the troposphere as a response to stratospheric impacts on baroclinic life cycles, Wittman et al. (2007) demonstrate how stratosphere-induced changes to life cycle behavior can act to modify the tropospheric annular mode. In particular, increased lower stratospheric shear is found to amplify the zonal mean response to LC1 life cycles, which in turn is associated with an amplification of a positive tropospheric annular mode signal, consistent with the observed stratosphere–troposphere connection. However, adding a stratospheric jet in our simulations within the LC1 regime does not amplify the response to LC1 life cycles (see, e.g., Fig. 3 or 8 at $U_{CS} = 4\ \mathrm{m\ s^{-1}}$, very similar to the response at $U_{CS} = 0\ \mathrm{m\ s^{-1}}$).

(ii) Wittman et al. (2007) find an LC1 to LC2 transition when the stratospheric shear is increased (i.e., for stronger stratospheric winds). In the context of stratosphere–troposphere coupling, this is in opposition to the results of the present study, with an LC2 to LC1 transition for stronger stratospheric winds, which suggests a stratosphere–troposphere connection consistent with observations, whereas Wittman et al. (2007) suggest the opposite. These differences may simply arise from the fact that our initial zonal flow setup is less simplified than that of Wittman et al. (2007), which instead allows for a close comparison with the linear analysis in that study, starting with the Eady problem of baroclinic instability.

Finally, we return to the relation between either kind of baroclinic wave life cycle (or wave breaking) and the phase of the NAO. To gain insight into the vertical structure of the NAO-like response (seen in Fig. 8), we compare vertical profiles of the zonal mean zonal wind from different life cycle simulations, averaged between 50° and 60° latitude. At these latitudes the largest meridional surface pressure and geopotential height gradients are found both in the response to idealized baroclinic wave life cycles (Fig. 8) and in the observed pattern of the NAO. The initial zonal wind profiles for S00T07.25 and S75T07.25 (Fig. 9) are, by construction, nearly identical in the troposphere but not in the

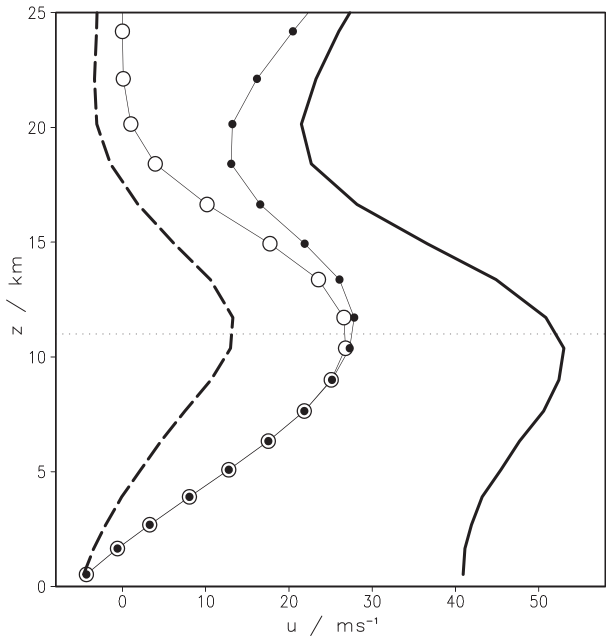

FIG. 9. Vertical profile of zonal mean zonal wind $\overline{u}$, averaged between 50° and 60° latitude of initial flow for S00T07.25 (thin line, open circles), initial flow for S75T07.25 (thin line, closed circles), flow after the barotropic decay stage of S00T07.25 (thick dashed line), and flow after the barotropic decay stage of S75T07.25 (thick solid line). An average over the last 5 days (t = 25, . . . , 30 days) is used in the latter two cases. The dotted line marks the tropopause at 11 km.

stratosphere. After the nonlinear life cycle is completed, however, the corresponding wind profiles differ significantly and the largest differences occur even in the troposphere: during the LC1 life cycle (S75T07.25), the zonal wind increases by 24 m s^{-1} near the tropopause and by 46 m s^{-1} at the surface. In contrast, during the LC2 life cycle (S00T07.25) the zonal wind decreases by 13 m s^{-1} near the tropopause but does not change at the surface. Hence, both life cycles reduce the initially strong vertical wind shear and thus the baroclinicity, but the changes due to anticyclonic wave breaking (LC1) are maximized at the surface, whereas the largest changes due to cyclonic wave breaking are found near the tropopause. Despite these differences in the response to an individual life cycle between lower and upper tropospheric levels, the difference between the two final responses (the difference between the thick lines in Fig. 9) depends only weakly on height throughout the troposphere. This further confirms the equivalent barotropic structure of a variability mode that may arise from the successive occurrence of AB and CB events.

This result closely resembles the picture of positive (negative)-phase NAO-like circulation dipoles reflecting the response to AB (CB) events at lower (upper) levels, suggested by Kunz et al. (2009). They study the synoptic evolution of AB and CB composites, computed from a large ensemble of such events in a forced-dissipative simulation with a simplified general circulation model. They find that CB events drive strong negative-phase NAO-like circulation dipoles in the upper troposphere but not at the surface, whereas AB events are found to drive strong positive phase NAO-like dipoles at the surface but not at upper levels, summarized by schematic vertical profiles of zonal wind (see their Fig. 10) similar to the profiles shown in Fig. 9 of this study. However, the very strong westerlies produced by the LC1 life cycle (thick solid line) are a specific outcome of the simulation of adiabatic and frictionless baroclinic wave life cycles. Clearly, surface friction would act to reduce the strong surface westerlies generated by the LC1 life cycle and by Ekman pumping also at upper tropospheric levels.

5. Conclusions and discussion

This model study investigates the response of baroclinic wave life cycles to different stratospheric flow conditions specified in the initial conditions of a series of adiabatic and frictionless life cycle simulations. A complete nonlinear baroclinic life cycle is initiated by a small-amplitude surface pressure perturbation of zonal wavenumber 6. Cyclonic shear, which is confined to the lower troposphere and centered about the unstable midlatitude tropospheric jet at 45° latitude, is added to the initial flow to control life cycle behavior. Beyond a critical value of the shear parameter that determines the strength of the initial shear, the simulations result in LC2 life cycles associated with cyclonic wave breaking rather than LC1 life cycles associated with anticyclonic wave breaking for small values of the shear parameter, similarly to Hartmann (2000). The shear parameter is used to bring the system close to the LC1–LC2 transition point. Wavenumber-5 (7) life cycles are found to result solely in LC1 (LC2) behavior. A stratospheric jet at different latitudinal positions is then included in the initial conditions and the response of the baroclinic life cycles is investigated. We conclude as follows:

- As the main result, a distinct stratosphere-induced shift of the LC1–LC2 transition point is obtained in the sense that larger initial cyclonic shear is necessary for the life cycles to evolve as LC2. Consequently, a stratosphere-sensitive regime (with respect to the shear parameter) exists, and within this regime a removal of the stratospheric jet induces an LC1 to LC2 transition.
- This stratosphere-sensitive regime is maximized when the stratospheric jet is located between 50° and 65° latitude, just where the observed stratospheric polar night

jet has its climatological position. The stratosphere-sensitive regime, though smaller, is also found when the stratospheric jet is located on the equatorward side of the tropospheric jet. Only a stratospheric jet at rather unrealistically low latitudes ($\leq$30° latitude) leads to a reversed life cycle response in the troposphere.

- The linear analysis of the stratosphere-induced changes, in terms of refractive index and fastest-growing normal mode structure, is found to be unable to explain the subsequent changes in life cycle behavior, although it may help to understand the larger stratosphere-sensitive regime obtained for a stratospheric jet at higher latitudinal positions.
- Consequently, stratosphere-induced changes of nonlinear wave–mean flow interactions must play an important role for the baroclinic response. Additional downward wave propagation (equatorward heat fluxes) between 14 and 18 km and 40° and 50° latitude, related to a shallow propagation region (with $\overline{q}_\phi < 0$ and $\overline{u} - ca\cos\phi < 0$) near 20 km, occurs when the stratospheric jet is removed, inducing an equatorward circulation near the tropopause. This feature extends far into the nonlinear baroclinic growth stage, independent of the latitudinal position of the stratospheric jet, and is probably involved in the nonlinear response, although future investigation is necessary to gain further insight into the mechanism.

Because (i) observational and modeling evidence exists that the positive (negative) phase of the NAO is driven by anticyclonic (cyclonic) wave breaking (Benedict et al. 2004; Franzke et al. 2004; Rivière and Orlanski 2007) and (ii) the difference between the LC1 and LC2 tropospheric circulation response is shown to closely resemble the meridional and vertical structure of the NAO, the above results immediately imply the possibility of a direct response of tropospheric baroclinic processes to the lower stratospheric flow to explain the observed connection between the stratospheric annular mode and the NAO.

This idea is basically similar to that of Wittman et al. (2007), although their results are discussed in the context of the Arctic Oscillation/annular mode instead of the NAO. However, there are essential differences compared to the present study, mainly arising from the different initial zonal flow conditions. Instead of adding a stratospheric polar night jet to the initial flow, Wittman et al. (2007) modify the vertical zonal wind shear above the tropopause among their different life cycle simulations. The advantage of this approach is that it allows for a close comparison with the linear analysis in that study, including the Eady problem of baroclinic instability with different lower stratospheric shear. However, although such linear considerations provide some insights into the dynamics of small-amplitude growing baroclinic waves under different stratospheric conditions, they are also unable to explain the main results of the nonlinear life cycle simulations of Wittman et al. (2007)—specifically, the amplification of the baroclinic wave development and subsequent zonal mean response within the LC1 regime as well as the LC1 to LC2 transition, both obtained for increased stratospheric shear.

In the above context of stratosphere–troposphere coupling, the transition in nonlinear life cycle behavior from LC1 to LC2 for increased stratospheric shear reported by Wittman et al. (2007) is the probably most important difference compared to the present study, where an opposite transition from LC2 to LC1 is obtained for stronger stratospheric winds. From the resulting zonal mean zonal wind changes in the troposphere, and also in the NAO–wave breaking view (see section 4), this result of Wittman et al. (2007) would contradict the observed stratosphere–troposphere connection.

However, the second relevant result of Wittman et al. (2007)—that is, the amplified tropospheric annular mode signal to increased stratospheric shear (and thus winds) within the LC1 regime—may serve as an additional mechanism for stratosphere–troposphere coupling. Whereas the LC1–LC2 transition found in the present study occurs at only one zonal wavenumber, the former mechanism may extend the coupling to the range of longer synoptic-scale waves, particularly during positive annular mode episodes when the tropospheric jet is expected to be in the LC1 regime and strong lower stratospheric winds may resemble the initial flow setup in Wittman et al. (2007) even more closely than the stratospheric jet used in our study or in Wittman et al. (2004). Certainly, this is highly speculative, but it also highlights the need for a deeper and thorough understanding of the nonlinear interaction of baroclinic waves with the lower stratosphere.

Finally, we note that Kunz et al. (2009) also find more (less) frequent AB (CB) events below a stronger stratospheric jet. However, from their forced-dissipative model simulations it is hardly possible to decide whether the obtained response follows from a direct modulation of tropospheric baroclinic waves or from an altered secondary circulation through changes in stratospheric wave forcing. To this end, the initial value approach of the present study appears as a particular advantage because by the balanced initial zonal flow and single zonal wavenumber the baroclinic response can clearly be attributed to a direct modulation by the stratospheric flow.

Acknowledgments. This work was funded by the Deutsche Forschungsgemeinschaft, Project SFB-512. Discussion with Christian Franzke, Martin Keller, and

Richard Greatbatch is greatly appreciated. Finally, we thank Steven Feldstein and two anonymous reviewers for their useful comments on the first draft of the manuscript.

APPENDIX

Setup of Balanced Initial Zonal Flow

The balancing procedure of obtaining the mass field that balances the prescribed initial zonal flow (1) essentially follows Hoskins and Simmons (1975; see their appendix). The model solves the nondimensional primitive equations in σ coordinates for the prognostic variables: absolute vorticity $\hat{\zeta} = \zeta\Omega^{-1}$, divergence $\hat{D} = D\Omega^{-1}$, temperature $\hat{T} = Ta^{-2}\Omega^{-2}R$ (R is the gas constant of dry air), and the logarithm of surface pressure $\ln\hat{p}^* = \ln(p^*p_0^{-1})$. By imposing the restrictions of zero meridional and vertical velocity and zero zonal variation and time tendencies on the model equations, the balance equation is obtained:

$$\underbrace{-\frac{\partial}{\partial\mu}(\hat{\zeta}\hat{U}) - \nabla^2\left[\frac{\hat{U}^2}{2(1-\mu^2)}\right]}_{\mathrm{F}} = \underbrace{\frac{\partial}{\partial\mu}\left[(1-\mu^2)\hat{T}\frac{\partial\ln\hat{p}^*}{\partial\mu}\right]}_{\mathrm{M1}} + \underbrace{\nabla^2\hat{\Phi}}_{\mathrm{M2}}, \tag{A1}$$

where $\mu = \sin\phi$, $\nabla^2 = \partial/\partial\mu[(1-\mu^2)\partial/\partial\mu]$, $\hat{\Phi} = \Phi a^{-2}\Omega^{-2}$ is the nondimensional geopotential, and $\hat{U} = ua^{-1}\Omega^{-1}(1-\mu^2)^{1/2}$ (so that $\hat{\zeta} = 2\mu - \partial\hat{U}/\partial\mu$). From (A1) $\hat{\Phi}$ is given by

$$\underbrace{\nabla^{-2}(F - \mathrm{M1})}_{\mathrm{Y}} = \hat{\Phi}. \tag{A2}$$

The hydrostatic equation $\hat{T} = -\partial\hat{\Phi}/\partial\ln\sigma$ may be expressed in the integrated and discretized form as $\mathbf{\Phi}_n = \mathbf{g}\mathbf{T}_n$, where $\mathbf{\Phi}_n$ and $\mathbf{T}_n$ are column vectors specifying the values of $\hat{\Phi}$ and $\hat{T}$, respectively, at each full level, n indicates the horizontal spectral mode ($n = 1, \ldots, 21$ represents the zonally uniform modes that are symmetric about the equator; $n = 0$ is the horizontal mean); and the matrix $\mathbf{g}$ is defined by $g_{ij} = \Delta\ln\sigma$ for $i < j$, $g_{ii} = 1 - (\sigma_{j-0.5}\Delta\ln\sigma/\Delta\sigma)$ for $i = j$, and $g_{ij} = 0$ for $i > j$, with $\Delta\sigma = \sigma_{j+0.5} - \sigma_{j-0.5}$ and $\Delta\ln\sigma = \ln\sigma_{j+0.5} - \ln\sigma_{j-0.5}$.[7] Using the same notation for Y, (A2) yields

$$\mathbf{g}^{-1}\mathbf{Y}_n = \mathbf{T}_n. \tag{A3}$$

In cases of zero initial zonal flow (1) at $z = 0$ (shear parameter $U_{\mathrm{CS}} = 0$), it is required that $\partial\ln\hat{p}^*/\partial\mu = 0$. Hence, Y is independent of $\ln\hat{p}^*$ and $\hat{T}$ can readily be obtained from (A3). In all other cases (shear parameter $U_{\mathrm{CS}} \neq 0$), it is required that $\partial\ln\hat{p}^*/\partial\mu \neq 0$ and, for a given surface pressure field, $\hat{T}$ is determined iteratively from (A3), using the start values $\mathbf{T}_{n>0} = 0$ and setting the profile $\mathbf{T}_0$ equal to the *U.S. Standard Atmosphere, 1976* (COESA 1976). Convergence is reached after less than 10 iterations.

A first-guess surface pressure field is obtained by numerical integration of the geostrophic wind relation at $\sigma = 1$:

$$\frac{\partial\ln\hat{p}^*}{\partial\mu} = -\frac{\mu}{1-\mu^2}\left(\frac{2\hat{U}}{\hat{T}^*} + \frac{1}{1-\mu^2}\frac{\hat{U}^2}{\hat{T}^*}\right), \tag{A4}$$

where $\hat{U}$ is approximated by $u|_{z=0}a^{-1}\Omega^{-1}(1-\mu^2)^{1/2}$ from (1) and the surface temperature $\hat{T}^*$ by numerical integration of the thermal wind relation (written in z) at $z = 0$; that is,

$$\frac{\partial\hat{T}^*}{\partial\mu} = -2H\frac{\mu}{1-\mu^2}\left(\frac{\partial\hat{U}}{\partial z} + \frac{1}{1-\mu^2}\hat{U}\frac{\partial\hat{U}}{\partial z}\right), \tag{A5}$$

where $\hat{U}$ is approximated as in (A4) and $\partial\hat{U}/\partial z$ by $(\partial u/\partial z)|_{z=0}a^{-1}\Omega^{-1}(1-\mu^2)^{1/2}$. The surface pressure field is then optimized to reduce large vertical two-grid oscillations by minimization of the cost function $bf = [\Sigma_{n=1}^{21}(\mathbf{A}^\top\mathbf{T}_n)^2]^{1/2}$, where $\mathbf{A}^\top = (1, -1, 1, \ldots)$. Optimization of only four surface pressure modes ($n = 1, \ldots, 4$) is found to be sufficient to obtain smooth temperature fields after less than 200 iterations of a downhill simplex method.

[7] Note that the matrix $\mathbf{g}$ differs from that in Hoskins and Simmons (1975).

REFERENCES

Ambaum, M. H. P., and B. J. Hoskins, 2002: The NAO troposphere–stratosphere connection. *J. Climate,* **15,** 1969–1978.

——, ——, and D. B. Stephenson, 2001: Arctic Oscillation or North Atlantic Oscillation. *J. Climate,* **14,** 3495–3507.

Andrews, D. G., J. R. Holton, and C. B. Leovy, 1987: *Middle Atmosphere Dynamics*. Academic Press, 489 pp.

Baldwin, M. P., and T. J. Dunkerton, 1999: Propagation of the Arctic Oscillation from the stratosphere to the troposphere. *J. Geophys. Res.,* **104,** 30 937–30 946.

——, and ——, 2001: Stratospheric harbingers of anomalous weather regimes. *Science,* **294,** 581–584.

——, X. Cheng, and T. J. Dunkerton, 1994: Observed correlations between winter-mean tropospheric and stratospheric circulation anomalies. *Geophys. Res. Lett.,* **21,** 1141–1144.

——, D. B. Stephenson, D. W. J. Thompson, T. J. Dunkerton, A. J. Charlton, and A. O'Neill, 2003: Stratospheric memory and skill of extended-range weather forecasts. *Science,* **301,** 636–640.

——, M. Dameris, and T. G. Shepherd, 2007: How will the stratosphere affect climate change? *Science,* **316,** 1576–1577.

Benedict, J. J., S. Lee, and S. B. Feldstein, 2004: Synoptic view of the North Atlantic Oscillation. *J. Atmos. Sci.,* **61,** 121–144.

Blessing, S., K. Fraedrich, M. Junge, T. Kunz, and F. Lunkeit, 2005: Daily North Atlantic Oscillation (NAO) index: Statistics and its stratospheric polar vortex dependence. *Meteor. Z.,* **14,** 763–769.

Canziani, P. O., and W. E. Legnani, 2003: Tropospheric–stratospheric coupling: Extratropical synoptic systems in the lower stratosphere. *Quart. J. Roy. Meteor. Soc.,* **129,** 2315–2329.

Charlton, A. J., A. O'Neill, W. A. Lahoz, and A. C. Massacand, 2004: Sensitivity of tropospheric forecasts to stratospheric initial conditions. *Quart. J. Roy. Meteor. Soc.,* **130,** 1771–1792.

COESA, 1976: *U.S. Standard Atmosphere, 1976*. NOAA, 277 pp.

Feldstein, S. B., 2003: The dynamics of NAO teleconnection pattern growth and decay. *Quart. J. Roy. Meteor. Soc.,* **129,** 901–924.

Fraedrich, K., E. Kirk, and F. Lunkeit, 1998: Portable University Model of the Atmosphere. Deutsches Klimarechenzentrum Tech. Rep. 16, 38 pp.

——, ——, U. Luksch, and F. Lunkeit, 2005: The Portable University Model of the Atmosphere (PUMA): Storm track dynamics and low-frequency variability. *Meteor. Z.,* **14,** 735–745.

Franzke, C., S. Lee, and S. B. Feldstein, 2004: Is the North Atlantic Oscillation a breaking wave? *J. Atmos. Sci.,* **61,** 145–160.

Hartmann, D. L., 2000: The key role of lower-level meridional shear in baroclinic wave life cycles. *J. Atmos. Sci.,* **57,** 389–401.

——, and P. Zuercher, 1998: Response of baroclinic life cycles to barotropic shear. *J. Atmos. Sci.,* **55,** 297–313.

Haynes, P. H., M. E. McIntyre, T. G. Shepherd, C. J. Marks, and K. P. Shine, 1991: On the "downward control" of extratropical diabatic circulations by eddy-induced mean zonal forces. *J. Atmos. Sci.,* **48,** 651–678.

Heifetz, E., C. H. Bishop, B. J. Hoskins, and J. Methven, 2004: The counter-propagating Rossby-wave perspective on baroclinic instability. I: Mathematical basis. *Quart. J. Roy. Meteor. Soc.,* **130,** 211–231.

Hoskins, B. J., and A. J. Simmons, 1975: A multi-layer spectral model and the semi-implicit method. *Quart. J. Roy. Meteor. Soc.,* **101,** 637–655.

Kunz, T., K. Fraedrich, and F. Lunkeit, 2009: Synoptic-scale wave breaking and its potential to drive NAO-like circulation dipoles: A simplified GCM approach. *Quart. J. Roy. Meteor. Soc.,* **135,** 1–19.

Kushner, P. J., and L. M. Polvani, 2004: Stratosphere–troposphere coupling in a relatively simple AGCM: The role of eddies. *J. Climate,* **17,** 629–639.

Labitzke, K., and H. van Loon, 1988: Associations between the 11-year solar cycle, the QBO and the atmosphere. Part I: The troposphere and stratosphere in the Northern Hemisphere in winter. *J. Atmos. Terr. Phys.,* **50,** 197–206.

Lorenz, D. J., and D. L. Hartmann, 2003: Eddy–zonal flow feedback in the Northern Hemisphere winter. *J. Climate,* **16,** 1212–1227.

Magnusdottir, G., and P. H. Haynes, 1996: Wave activity diagnostics applied to baroclinic wave life cycles. *J. Atmos. Sci.,* **53,** 2317–2353.

Matsuno, T., 1970: Vertical propagation of stationary planetary waves in the winter Northern Hemisphere. *J. Atmos. Sci.,* **27,** 871–883.

——, 1971: A dynamical model of the stratospheric sudden warming. *J. Atmos. Sci.,* **28,** 1479–1494.

Methven, J., B. J. Hoskins, E. Heifetz, and C. H. Bishop, 2005: The counter-propagating Rossby-wave perspective on baroclinic instability. Part IV: Nonlinear life cycles. *Quart. J. Roy. Meteor. Soc.,* **131,** 1425–1440.

Orlanski, I., 2003: Bifurcation in eddy life cycles: Implications for storm track variability. *J. Atmos. Sci.,* **60,** 993–1023.

Perlwitz, J., and H.-F. Graf, 1995: The statistical connection between tropospheric and stratospheric circulation of the Northern Hemisphere in winter. *J. Climate,* **8,** 2281–2295.

——, and N. Harnik, 2003: Observational evidence of a stratospheric influence on the troposphere by planetary wave reflection. *J. Climate,* **16,** 3011–3026.

Polvani, L. M., and P. J. Kushner, 2002: Tropospheric response to stratospheric perturbations in a relatively simple general circulation model. *Geophys. Res. Lett.,* **29,** 1114, doi:10.1029/2001GL014284.

Rivière, G., and I. Orlanski, 2007: Characteristics of the Atlantic storm-track activity and its relation with the North Atlantic Oscillation. *J. Atmos. Sci.,* **64,** 241–266.

Scaife, A. A., J. R. Knight, G. K. Vallis, and C. K. Folland, 2005: A stratospheric influence on the winter NAO and North Atlantic surface climate. *Geophys. Res. Lett.,* **32,** L18715, doi:10.1029/2005GL023226.

Simmons, A. J., and B. J. Hoskins, 1980: Barotropic influences on the growth and decay of nonlinear baroclinic waves. *J. Atmos. Sci.,* **37,** 1679–1684.

——, and D. Burridge, 1981: An energy and angular-momentum conserving vertical finite-difference scheme and hybrid vertical coordinates. *Mon. Wea. Rev.,* **109,** 758–766.

Thompson, D. W. J., and J. M. Wallace, 1998: The Arctic Oscillation signature in the wintertime geopotential height and temperature fields. *Geophys. Res. Lett.,* **25,** 1297–1300.

——, M. P. Baldwin, and J. M. Wallace, 2002: Stratospheric connection to Northern Hemisphere wintertime weather: Implications for prediction. *J. Climate,* **15,** 1421–1428.

——, J. C. Furtado, and T. G. Shepherd, 2006: On the tropospheric response to anomalous stratospheric wave drag and radiative heating. *J. Atmos. Sci.,* **63,** 2616–2629.

Thorncroft, C. D., B. J. Hoskins, and M. E. McIntyre, 1993: Two paradigms of baroclinic-wave life-cycle behaviour. *Quart. J. Roy. Meteor. Soc.,* **119,** 17–55.

Ulbrich, U., and P. Speth, 1991: The global energy cycle of stationary and transient atmospheric waves—Results from ECMWF analyses. *Meteor. Atmos. Phys.,* **45,** 125–138.

Wittman, M. A. H., L. M. Polvani, R. K. Scott, and A. J. Charlton, 2004: Stratospheric influence on baroclinic life cycles and its connection to the Arctic Oscillation. *Geophys. Res. Lett.,* **31,** L16113, doi:10.1029/2004GL020503.

——, A. J. Charlton, and L. M. Polvani, 2007: The effect of lower stratospheric shear on baroclinic instability. *J. Atmos. Sci.,* **64,** 479–496.

Woollings, T., B. Hoskins, M. Blackburn, and P. Berrisford, 2008: A new Rossby wave–breaking interpretation of the North Atlantic Oscillation. *J. Atmos. Sci.,* **65,** 609–626.